Electronic Supplementary Information (ESI)

Synergistic electronic structure modulation of Pt using V_2O_3 and V_8C_7 for enhanced deuterium evolution performance

Yanfeng Li†, Yuan Sheng†, Liangbin Shao, Yuanan Li, Weiwei Xu, Shijie Zhang, Fangjun Shao, and Jianguo Wang**

Institute of Industrial Catalysis, College of Chemical Engineering, State Key Laboratory Breeding Base of Green-Chemical Synthesis Technology, Zhejiang University of Technology, Hangzhou 310032 China.

†Y.F. Li and Y. Sheng contribute to this work equally

*Correspondence and requests for materials should be addressed to F.J.S (email: shaofj@zjut.edu.cn), or to J.G.W (email: jgw@zjut.edu.cn).

1. Experimental section

1.1 Materials

Glucose ($C_6H_{12}O_6$, 99%, AR), ammonium metavanadate (NH_4VO_3, 99%, AR), and platinum (II) acetylacetonate ($Pt(acac)_2$, 97%) were purchased from McLean Chemical Reagent Co., Ltd. Potassium hydroxide (KOH, 95%), Sodium hydroxide (NaOH, 95%), and Deuterosulfuric acid (D_2SO_4, 99.5%) were obtained from Macklin Biochemical Co., Ltd. Perchloric acid ($HClO_4$, 70-72%), Cupric sulfate ($CuSO_4·5H_2O$, 99%), Sulfuric acid (H_2SO_4, 95-98%) and Sodium (Na, 99.5%) was purchased from Sinopharm Chemical Reagent Co., Ltd. Deuterated water (D_2O, 99.9%) was obtained from Shenzhen Ruilin Technology Co., Ltd. Nitrogen (N_2, 99.99%) is provided by Hangzhou Jingong Gas Co., Ltd. Commercial Pt/C (20 wt.%) was purchased from Alfa Aesar (China) Chemical Co., Ltd. Iridium oxide (IrO_2, SIr85), and Platinum-plated titanium felt, hydrophobic carbon paper (YLS 30T), and proton exchange membrane (Nafion 115, DuPont) were purchased from Suzhou Shengerno Technology Co., Ltd. Carbon cloth (W0S1011 Hydrophilic carbon cloth) were purchased from Carbon Energy Technology Co., Ltd. Ethanol (super dry, water < 50 ppm) was purchased from Meryer Co., Ltd. Deionized water was prepared using the HHitch laboratory water purification system. All chemicals were used as received, without further purification.

1.2 Synthesis of catalysts

A mixture of 50 mL of deionized water, 1 g of glucose, and 0.5 g NH_4VO_3 was subjected to ultrasonic treatment for 30 min until a transparent solution was obtained. The solution was transferred into a 100 mL PTFE-lined stainless-steel reaction vessel and sealed. The vessel was then heated at 160 °C for 15 h in an electrical oven and cooled to room temperature naturally. The resulting slurry

was subjected to suction filtration. The precipitate was washed with deionized water and ethanol, and vacuum dried at 60 °C for 12 hours. The dry solid was ground into a powder with mortar and pestle, followed by carbonization in a tube furnace where a 50 mL min^{-1} flow of Ar was used to protect the sample from oxidation. The heating rate was 5 °C min^{-1}, and the holding time was 3 hours after 900 °C was reached. The as-synthesized V_2O_3/V_8C_7 catalyst support was cooled to room temperature in the furnace with continuous supply of Ar.

The $Pt/V_2O_3/V_8C_7$ catalyst with a nominal Pt loading of 7 wt. % was prepared by wet impregnation. Typically, 14.1 mg of $Pt(acac)_2$, 100 mg of V_2O_3/V_8C_7, and 1 mL of ethanol were mixed, then and ground in an agate mortar. The slurry was dried under an infrared lamp. The resulting powder was annealed in flowing Ar at 350 °C for 3 hours with a heating rate of 5 °C min^{-1} and cooled to room temperature in the Ar stream.

Pt/V_2O_3 and Pt/V_8C_7 were synthesized by the same method, except that the amount of glucose was adjusted to 0.5 g and 2.0 g, respectively.

To synthesize Pt catalysts supported on glucose-derived carbon (Pt/GC), the same method as used for $Pt/V_2O_3/V_8C_7$ was followed except that no NH_4VO_3 was added.

1.3 Preparation of working electrode:

4 mg of catalyst powder was added into a mixture of 0.9 mL of absolute ethanol and 0.1 mL of 5 wt.% Nafion solution. The suspension was then sonicated for 30 min at room temperature to form the catalyst ink. The working electrode was prepared by drop-casting 1 mL of catalyst ink onto a 1 × 1 cm^2 carbon cloth under an infrared lamp.

1.4 Materials characterization

Field emission scanning electron microscopy (FE-SEM, HITACHI Regulus 8100) was performed at an acceleration voltage of 20 kV. Transmission electron microscopy (TEM, Tecnai G2F30S-Twin) images were obtained at 300 kV with samples drop-cast on carbon-coated Cu grids. Powder X-ray diffraction (XRD, Bruker D8 Advance) was carried out with Cu-Kα radiation (40 kV and 40 mA, λ = 0.1544 nm). X-ray photoelectron spectroscopy (XPS, Thermo Scientific ESCALAB 250 Xi) was performed with Al Kα radiation. Charge correction of the XPS data was made by setting the 1 s binding energy value of adventitious carbon at 284.8 eV. N_2 adsorption/desorption measurements were obtained on a Micromeritics ASAP2460 analyzer.

1.5 Electrochemical measurements

The electrochemical measurements were carried out by a CHI660D (CH Instruments, Inc., Shanghai) electrochemical workstation at room temperature. A standard three-electrode cell was used with a graphite rod electrode as the counter electrode (CE), a Hg/HgO electrode filled with 1 M KOH as reference electrode (RE) in alkaline solutions and a Ag/AgCl electrode filled with saturated KCl as RE in acidic solutions. The potential was converted to the scale with respect to reversible hydrogen electrode (RHE) using the following equations:

E(RHE)= E(Hg/HgO) + 0.097 V + 0.059×pH.

E(RHE)= E(Ag/AgCl) + 0.197 V + 0.059×pH.

Linear sweep voltammetry (LSV) measurements on catalytic activity were performed at a scan rate of 5 mV s^{-1}(with 85% iR compensation). Hydrogen underpotential deposition (UPD) was measured in 0.1 M $HClO_4$ and copper UPD/stripping in a mixed solution containing 0.05 M H_2SO_4 and 0.05 M $CuSO_4$. All the UPD experiments were carried out at a scan rate of 5 mV s^{-1} under

continuous bubbling of N_2. The electrolytes were deaerated with N_2 for 30 min in advance. Faradaic efficiency of DER/HER was determined by galvanostatic electrolysis where the volume of gas collected by the water displacement method was compared to the theoretical volume predicted by the Faraday's law.

1.6 PEM electrolysis

The membrane electrode assemblies (MEA) used in the PEM electrolyzer adopted the porous transport electrode (PTE) configuration. The anode PTE was based on Pt-plated Ti felt (0.4 mm thick with 5 μm of Pt coating), and the cathode PTE on commercial carbon paper (YLS 30T). To prepare the anode PTE, 10 mg of IrO_2 and 20 μL of 5 wt. % Nafion solution were dispersed in a mixture of 2 mL of isopropanol, 2 mL of anhydrous ethanol, and 1 mL of deionized water by sonication to form the catalyst ink. The ink was air-brushed onto the Pt-plated Ti felt to reach a loading of 6 mg cm^{-2}. The cathode was similarly prepared using commercial 20 wt. % Pt/C or $Pt/V_2O_3/V_8C_7$ as the catalyst at the loading of 4 mg cm^{-2} on the carbon paper. Finally, the PTEs and PEM were hot pressed together at 80 ℃ and 0.8 MPa for 4 min to form the MEA.

The MEA with a catalyst-coated area of 2 cm^2 on both anode and cathode was assembled into an in-house PEM electrolyzer consisting of a Ti anode plate, a SS316 cathode plate, and fluoroelastomer gaskets with thicknesses of 0.3 mm and 0.15 mm to seal the anode and cathode, respectively. Serpentine flow fields with a channel width of 1.2 mm were machined into the anode/cathode plates. During operation, the electrolyzer was kept at 80 ℃ by heating cartridges inserted into the middle of the anode/cathode plates. D_2O or deionized water was maintained at 80 ℃ in a jacketed glass vessel by recirculating hot water in the heating jacket. D_2O/H_2O was fed to the

electrolyzer by a peristaltic pump at approximately 0.72 mL min^{-1} on both the anode and cathode sides.

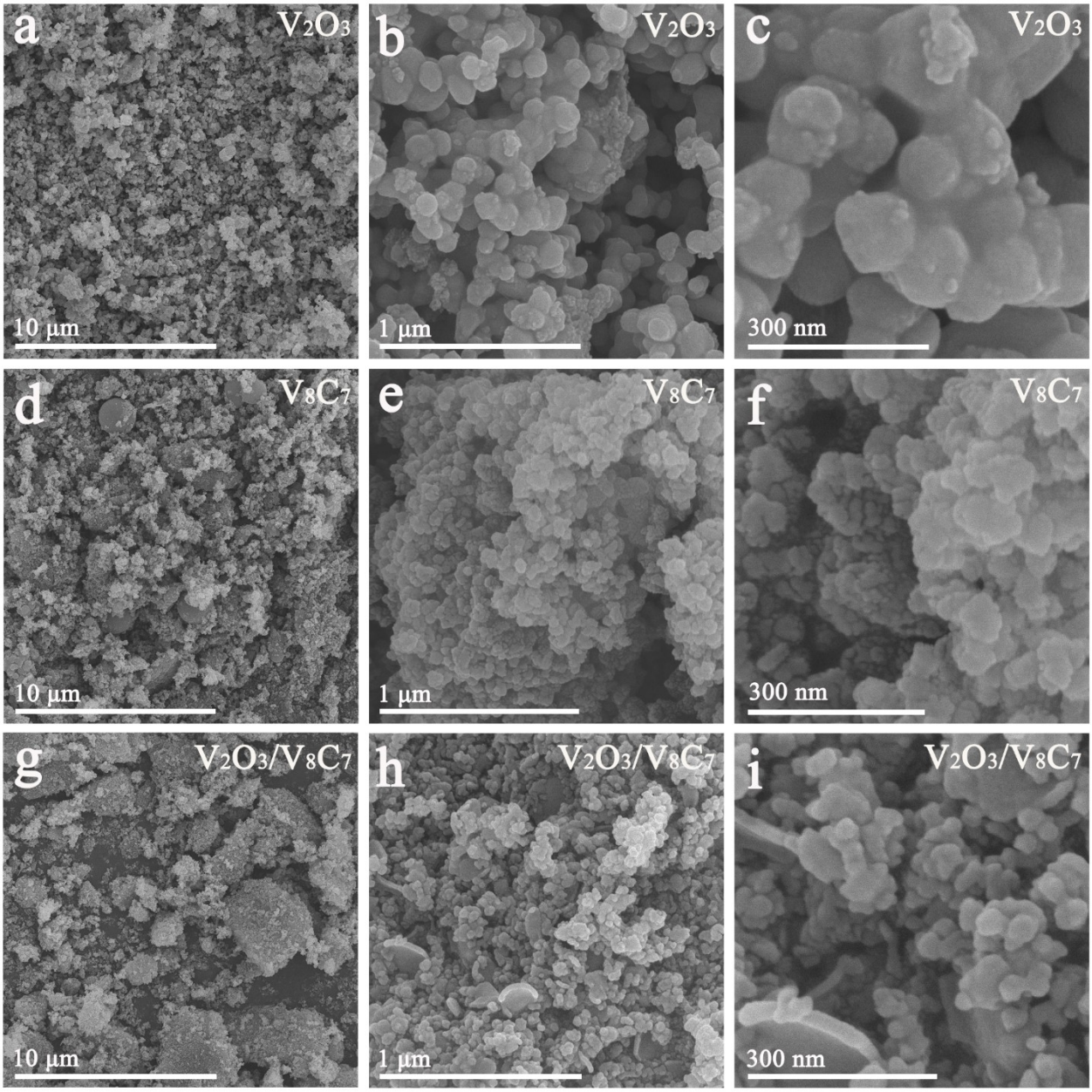

Figure S1. High-resolution SEM image of V_2O_3, V_8C_7, and V_2O_3/V_8C_7.

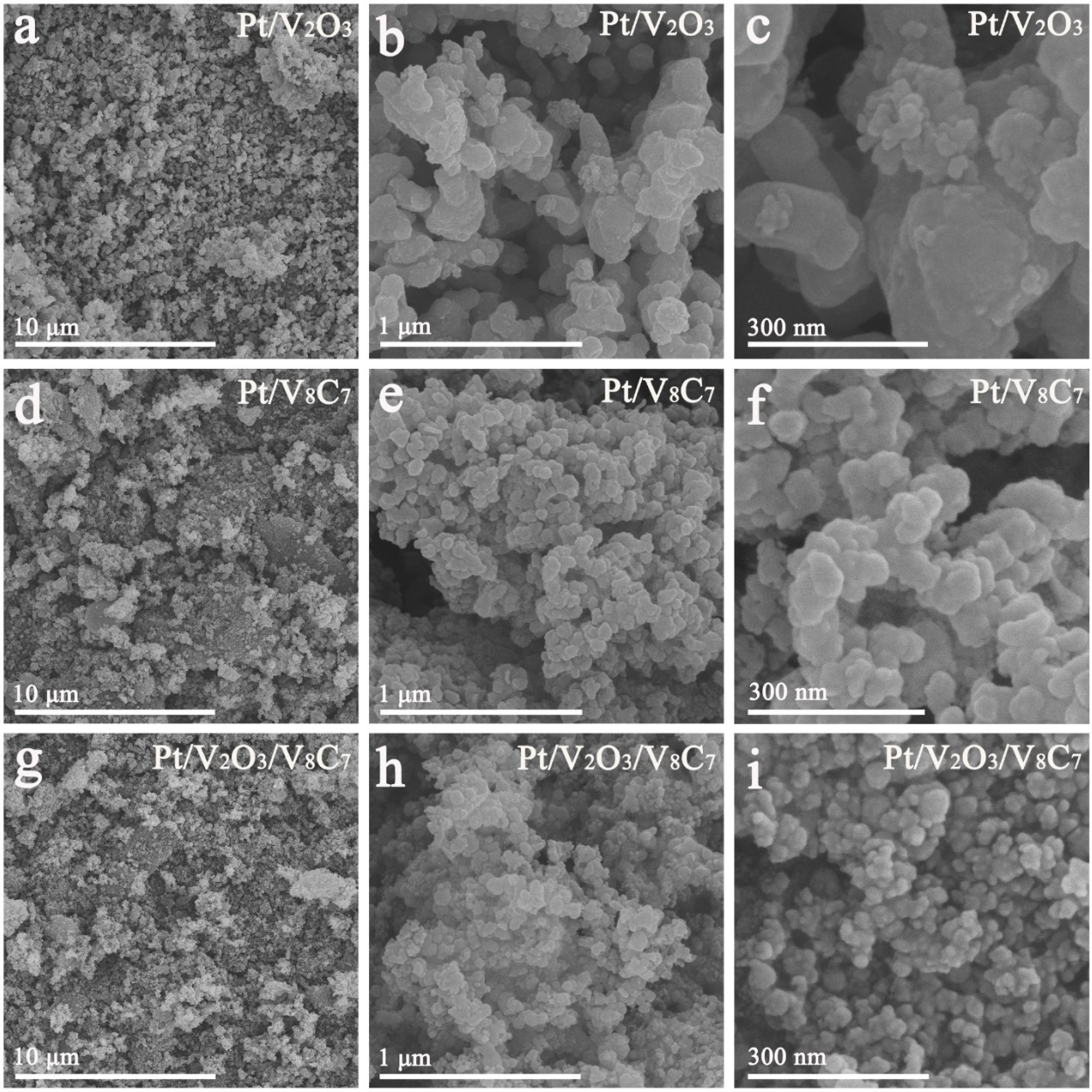

Figure S2. High-resolution SEM image of Pt/V_2O_3, Pt/V_8C_7, and $Pt/V_2O_3/V_8C_7$.

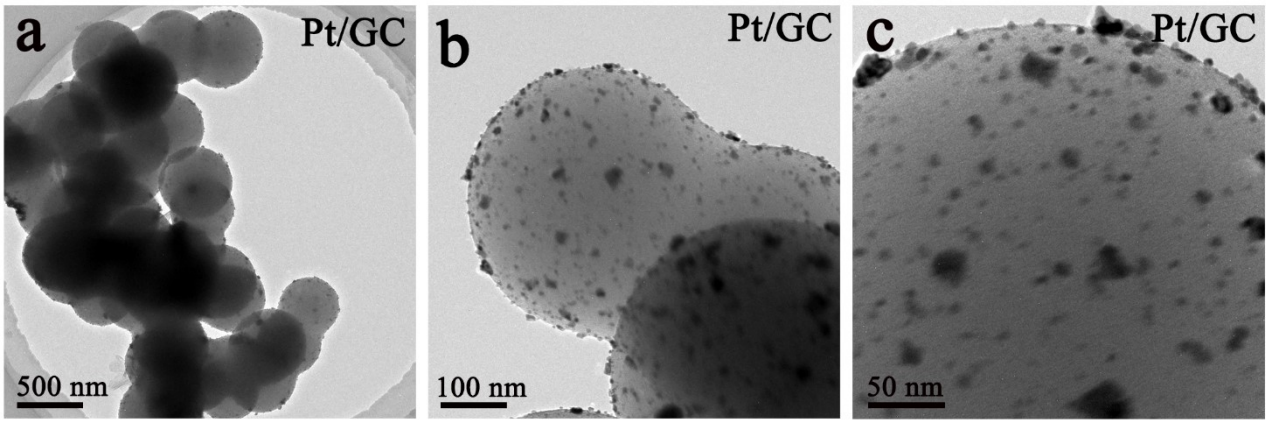

Figure S3. TEM image of Pt/GC.

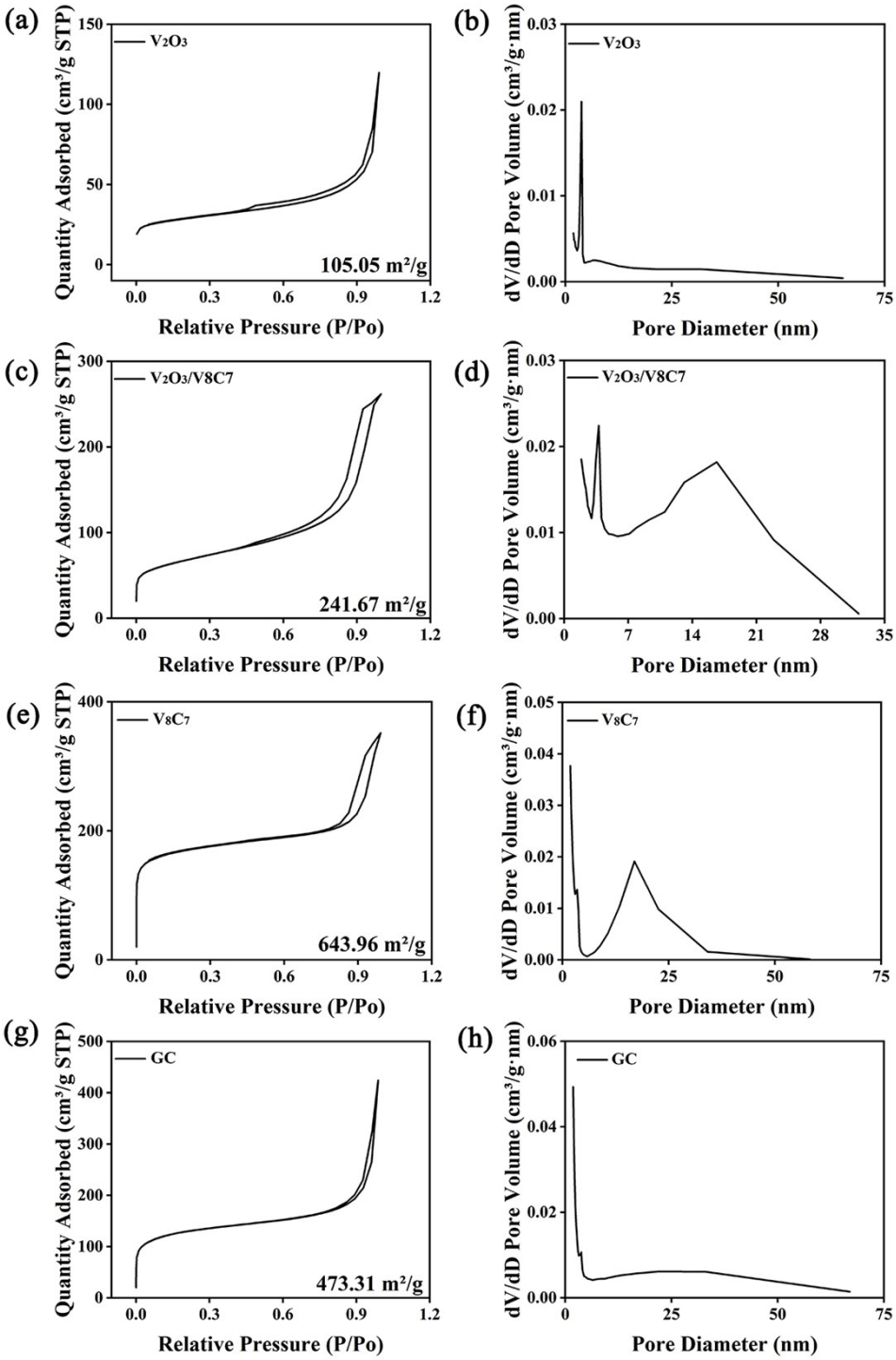

Figure S4. N_2 adsorption-desorption isotherms and pore size distribution of the support materials.

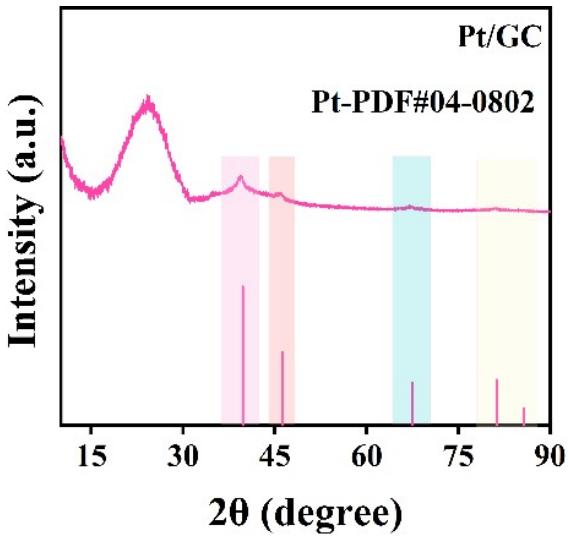

Figure S5. XRD pattern of Pt/GC.

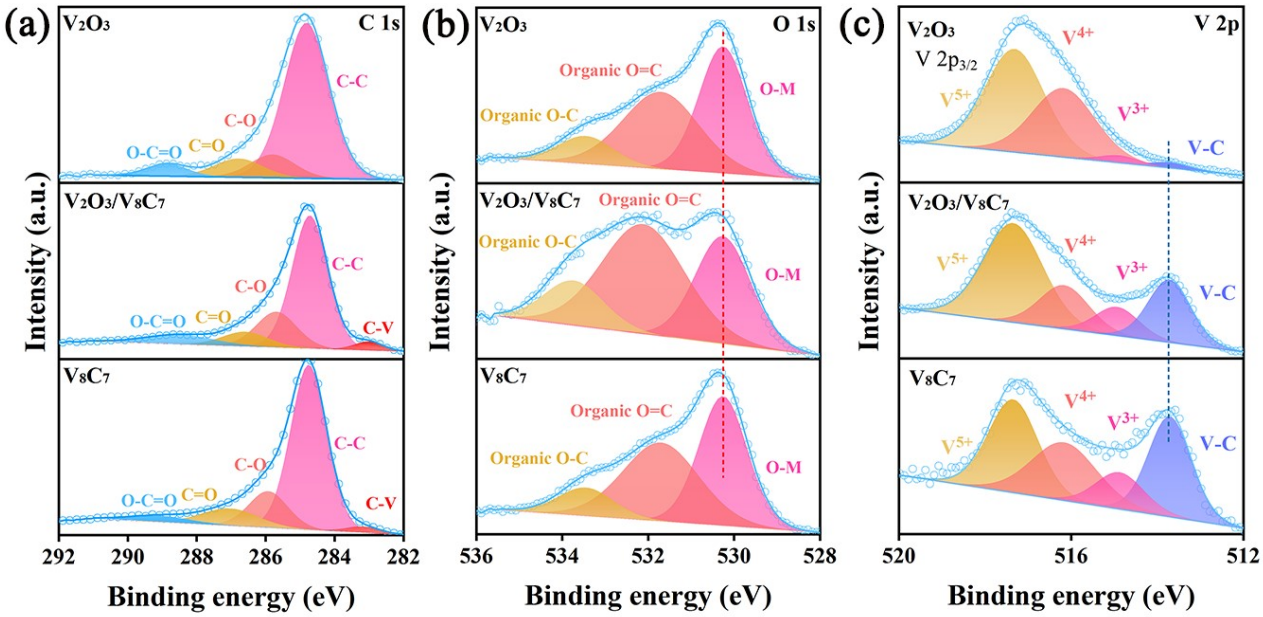

Figure S6. High-resolution XPS spectra of V_2O_3, V_2O_3/V_8C_7, and V_8C_7 in the (a) C1s, (b) V 2p, and (c) O1s regions.

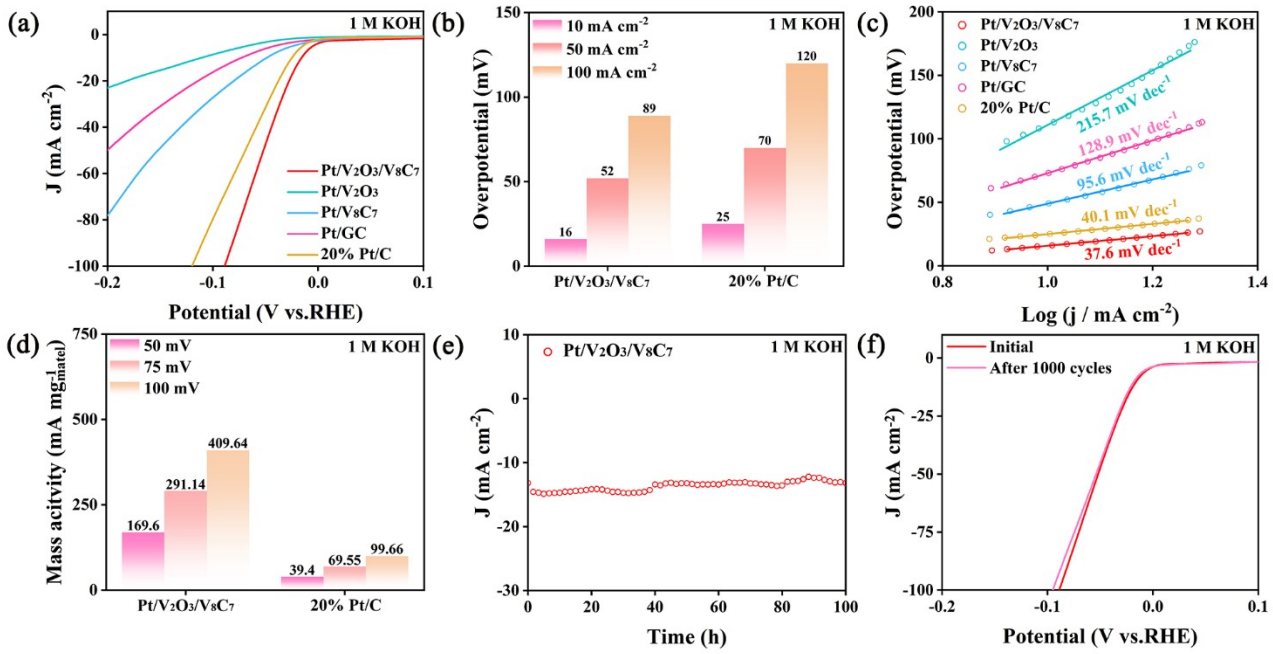

Figure S7. HER performance of $Pt/V_2O_3/V_8C_7$, Pt/V_2O_3, Pt/V_8C_7, Pt/GC, and 20% Pt/C in 1 M KOH. (a) LSV curves. (b) Overpotential at current densities of 10 mA cm^{-2}, 50 mA cm^{-2}, and 100 mA cm^{-2}. (c) Tafel plots. (d) Mass activity based on amount of Pt. (e) Long-term durability test and (f) accelerated durability test of $Pt/V_2O_3/V_8C_7$.

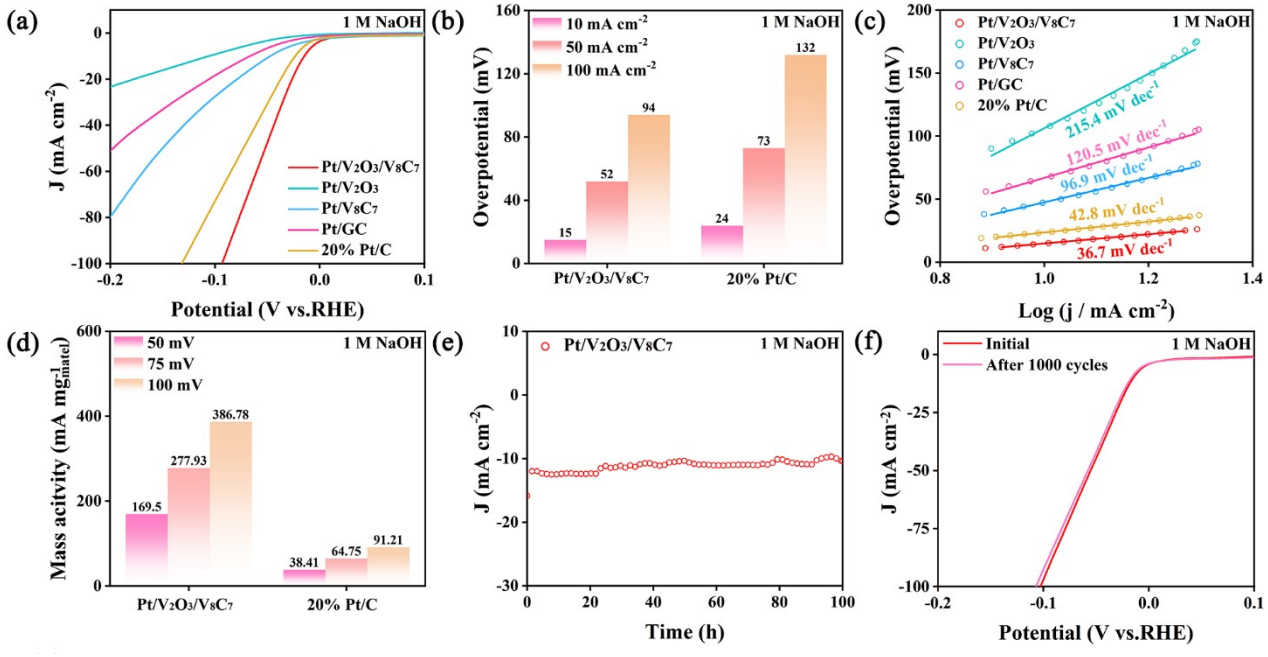

Figure S8. HER performance of $Pt/V_2O_3/V_8C_7$, Pt/V_2O_3, Pt/V_8C_7, Pt/GC, and 20% Pt/C in 1 M NaOH. (a) LSV curves. (b) Overpotential at current densities of 10 mA cm^{-2}, 50 mA cm^{-2}, and 100 mA cm^{-2}. (c) Tafel plots. (d) Mass activity based on amount of Pt. (e) Long-term durability test and (f) accelerated durability test of $Pt/V_2O_3/V_8C_7$.

Tabel S1. Comparison of overpotential required to achieve 10 mA cm^{-2} in alkaline electrolytes

Catalyst	**Overpotential at 10 mA cm^{-2}**		
	1 M NaOD	**1 M KOH**	**1 M NaOH**
$Pt/V_2O_3/V_8C_7$	37 mV	16 mV	15 mV
Pt/V_2O_3	180 mV	111 mV	107 mV
Pt/V_8C_7	95 mV	49 mV	48 mV
Pt/GC	130 mV	73 mV	67 mV
20% Pt/C	47 mV	25 mV	24 mV

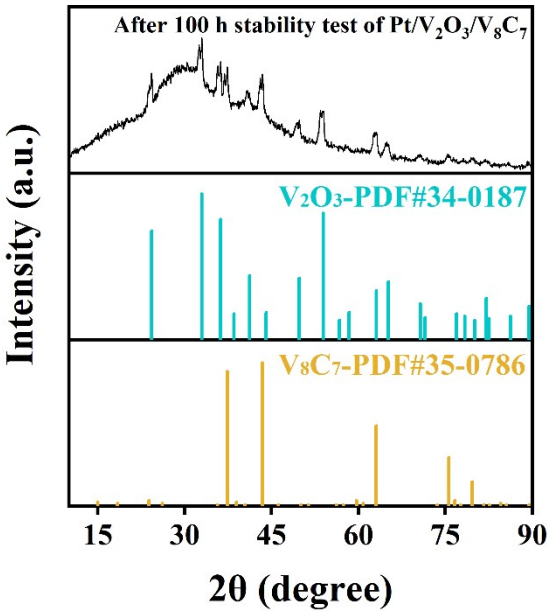

Figure S9. XRD pattern of $Pt/V_2O_3/V_8C_7$ after 100 h stability test (in 1 M NaOD).

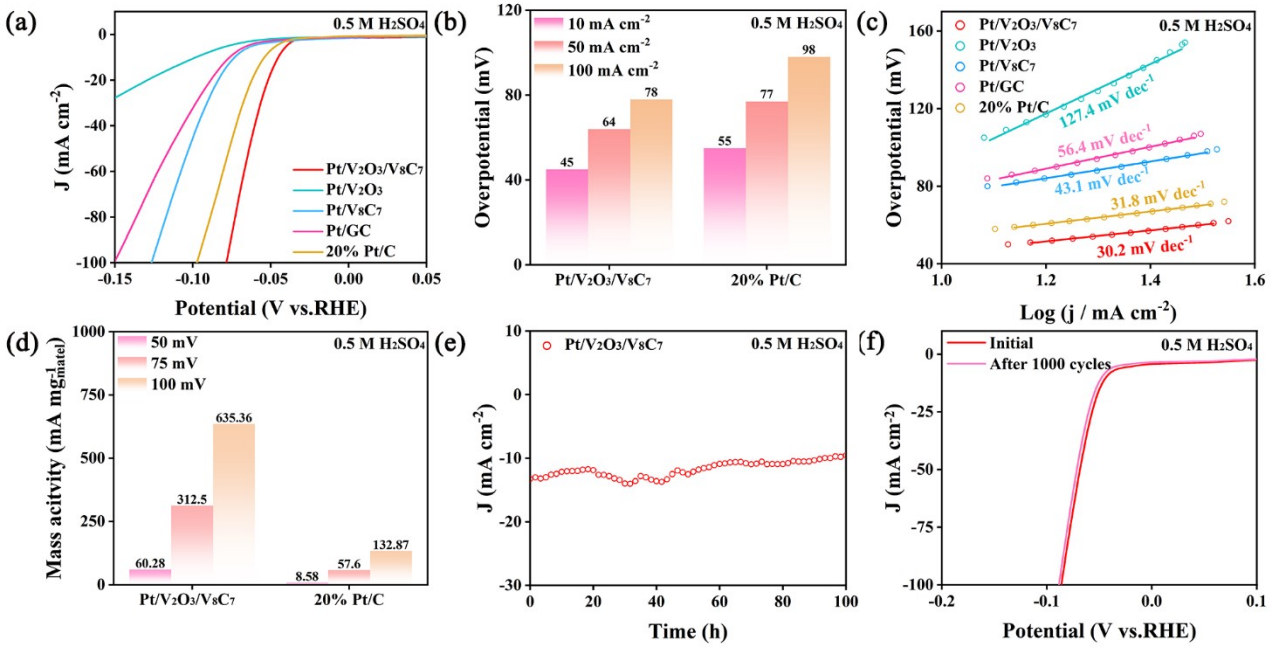

Figure S10. HER performance of $Pt/V_2O_3/V_8C_7$, Pt/V_2O_3, Pt/V_8C_7, Pt/GC, and 20% Pt/C in 0.5 M H_2SO_4. (a) LSV curves. (b) Overpotential at current densities of 10 mA cm^{-2}, 50 mA cm^{-2}, and 100 mA cm^{-2}. (c) Tafel plots. (d) Mass activity based on amount of Pt. (e) Long-term durability test and (f) accelerated durability test of $Pt/V_2O_3/V_8C_7$.

Tabel S2. Comparison of overpotential required to achieve 10 mA cm^{-2} in acidic electrolytes

Catalyst	**Overpotential at 10 mA cm^{-2}**	
	0.5 M D_2SO_4	**0.5 M H_2SO_4**
$Pt/V_2O_3/V_8C_7$	49 mV	45 mV
Pt/V_2O_3	129 mV	99 mV
Pt/V_8C_7	82 mV	74 mV
Pt/GC	92 mV	77 mV
20% Pt/C	63 mV	55 mV

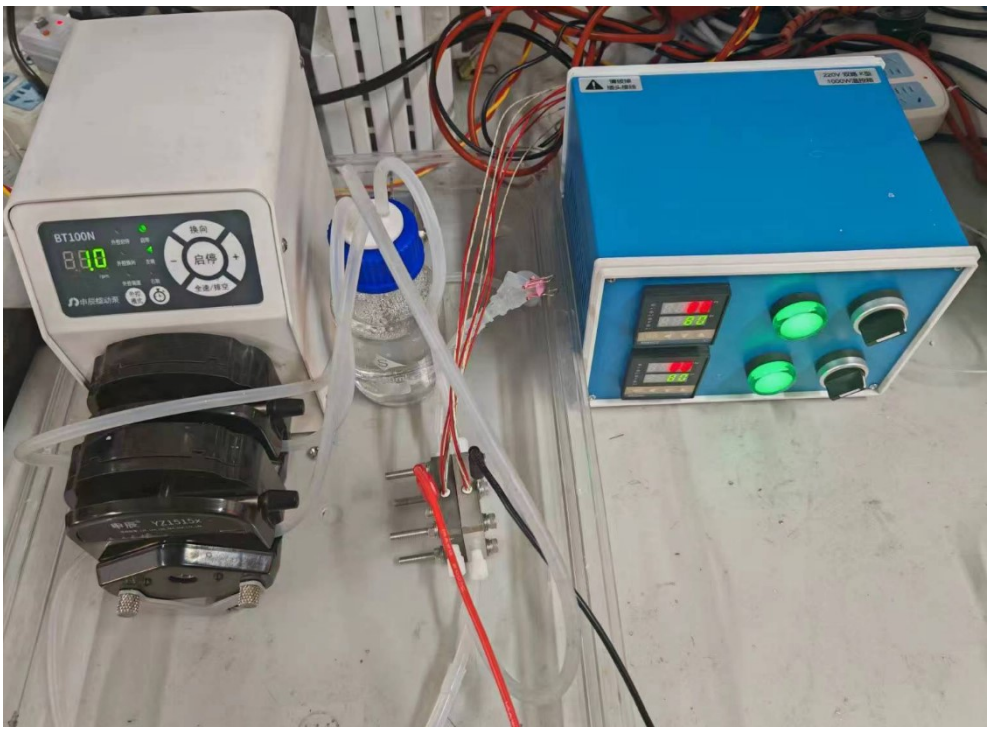

Figure S11. Photograph of the set-up for PEM electrolysis tests.

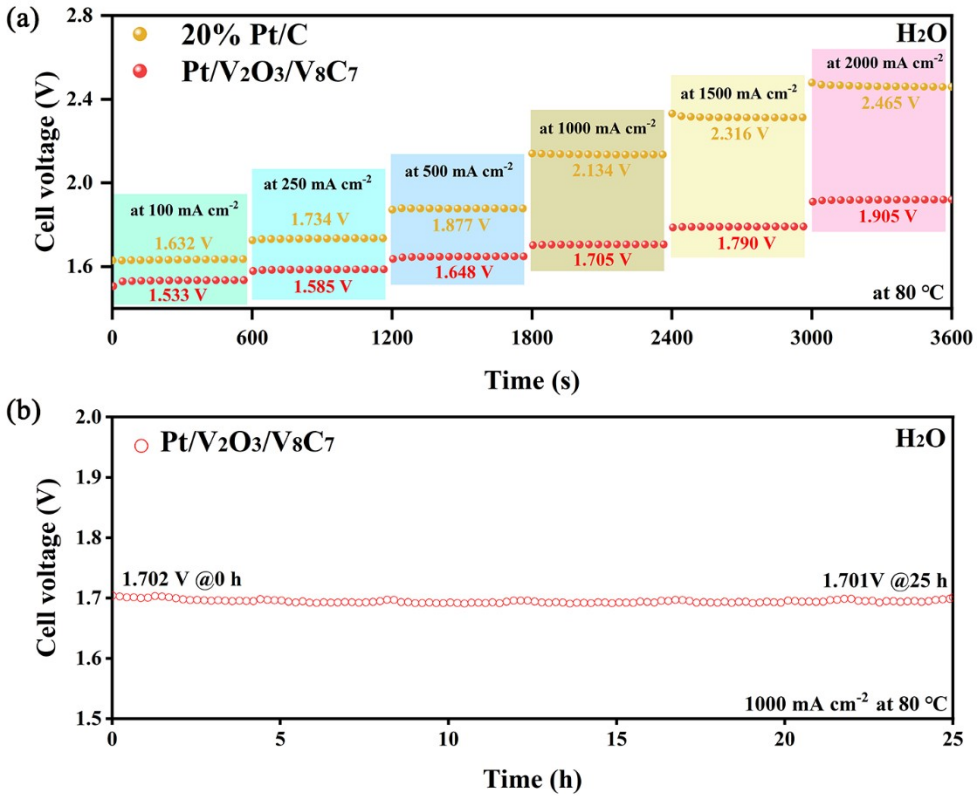

Figure S12. PEM electrolysis of H_2O. (a) Cell voltage at different current densities. (b) Stability test.

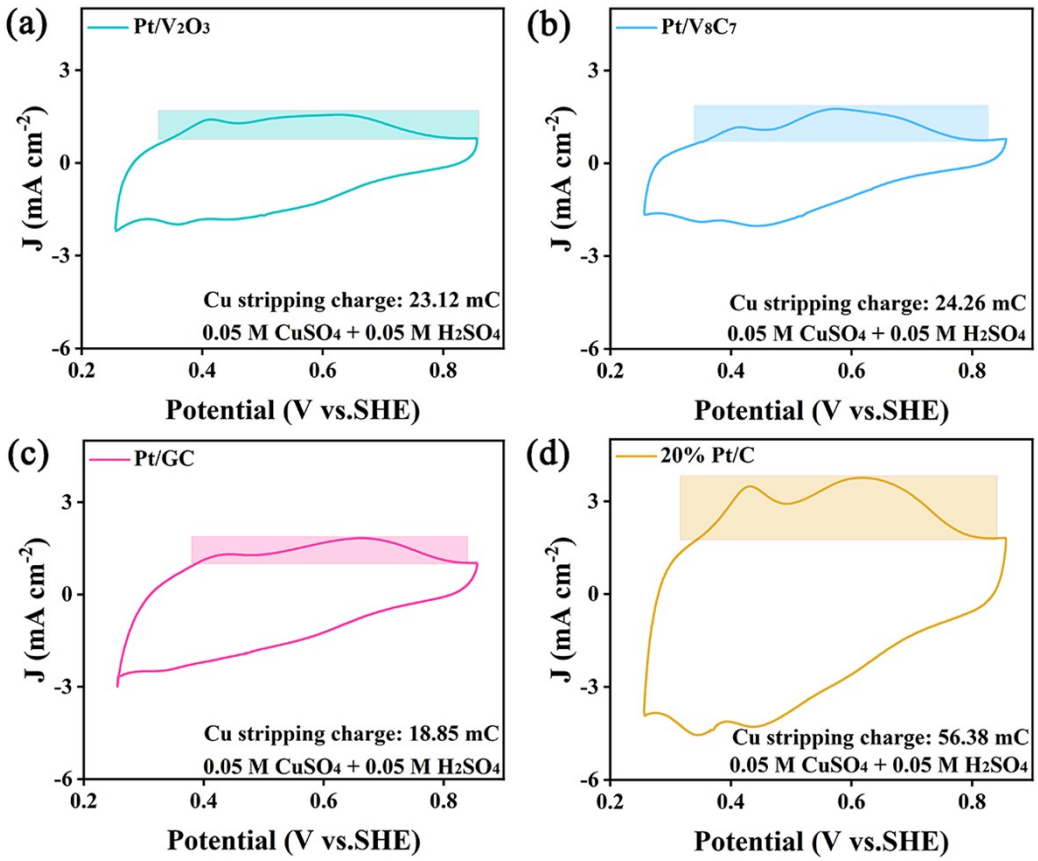

Figure S13. Underpotential deposition-stripping of Cu on Pt/V_2O_3, Pt/V_8C_7, Pt/GC, and 20% Pt/C.

Table S3. HER performance of $Pt/V_2O_3/V_8C_7$ and other reported Pt-based electrocatalysts in 1 M KOH.

Catalysts	Electrolyte	Overpotential at 10 mA cm^{-2} (mV)	Tafel slope (mV dec^{-1})	Ref.
$Pt/V_2O_3/V_8C_7$	**1 M KOH**	**16**	**37.6**	**This work**
Pt/NiCo@C	1M KOH	48	130	Ref.1[1]
Pt/WO3	1M KOH	8	35	Ref.2[2]
Pt-Co/CoO_x	1M KOH	28	29.3	Ref.3[3]
PtNi-NC-900	1M KOH	37.4	43.2	Ref.4[4]
d-Pt-Ni NWs	1M KOH	15	29	Ref.5[5]
10% NiOx@Pt/G	1M KOH	38.3	116	Ref.6[6]
Pt@Ni−Ni(OH)	1M KOH	27	50.7	Ref.7[7]
PtNiP-0.11 NWs	1M KOH	12	26.6	Ref.8[8]
Pt/NiFe-ED (300 μM)	1M KOH	17	45	Ref.9[9]
Pt_2Ni_3-PNWs	1M KOH	44	66	Ref.10[10]

Table S4. HER performance of $Pt/V_2O_3/V_8C_7$ and other reported Pt-based electrocatalysts in 0.5 M H_2SO_4.

Catalysts	Electrolyte	Overpotential at 10 mA cm^{-2} (mV)	Tafel slope (mV dec^{-1})	Ref.
$Pt/V_2O_3/V_8C_7$	**0.5 M H_2SO_4**	**45**	**30.2**	**This work**
PtSA-MIL100(Fe)	0.5 M H_2SO_4	60	31.16	Ref.11[11]
Pt-x -PVA	0.5 M H_2SO_4	34	31	Ref.12[12]
Pt-520/Au@MnO_2	0.5 M H_2SO_4	34	19	Ref.13[13]
Pt/NC-850	0.5 M H_2SO_4	17	32	Ref.14[14]
Pt-MoS_2	0.5 M H_2SO_4	67.4	76.2	Ref.15[15]
Pt/NP-CNTs	0.5 M H_2SO_4	25	28	Ref.16[16]
Pt/MIL-100(Fe)	0.5 M H_2SO_4	46	19.7	Ref.17[17]
$Pt_{61}La_{39}$@KB	0.5 M H_2SO_4	38	29	Ref.18[18]
Pt/Sv-MoS_{2-x}	0.5 M H_2SO_4	26.6	34.8	Ref.19[19]
Pt_1Ru_1/NMHCS-A	0.5 M H_2SO_4	22	38	Ref.20[20]

References

1. N. Chauhan, H. W. Choi, M. Kumar and D. H. Yoon, *Electrochim. Acta*, 2023, **460**, 142634.
2. X. Fan, C. Liu, B. Gao, H. Li, Y. Zhang, H. Zhang, Q. Gao, X. Cao and Y. Tang, *Small*, 2023, **19**, 2301178.
3. Y. Wang, W. Wu, R. Chen, C. Lin, S. Mu and N. Cheng, *Nano Res.*, 2022, **15**, 4958-4964.
4. J. Guo, J. Liu, X. Zhang, X. Guan, M. Zeng, J. Shen, J. Zou, Q. Chen, T. Wang and D. Qian, *J. Mater. Chem. A*, 2022, **10**, 13727-13734.
5. Y. Xie, J. Cai, Y. Wu, X. Hao, Z. Bian, S. Niu, X. Yin, Z. Pei, D. Sun, Z. Zhu, Z. Lu, D. Niu and G. Wang, *ACS Mater. Lett.*, 2021, **3**, 1738-1745.
6. F. Kwofie, Y. Cheng, R. Zhang and H. Tang, *Mater. Today Sustain.*, 2022, **19**, 100170.
7. D. Li, F. Liu, J. Dou and Q. Zhao, *ChemCatChem*, 2021, **13**, 5078-5083.
8. W. Lai, p. Yu, L. Gao, Z. Yang, B. He and H. Huang, *J. Mater. Chem. A*, 2022, **10**, 16834-16841.
9. Y. Feng, R. Ma, M. Wang, J. Wang, T. Sun, L. Hu, J. Zhu, Y. Tang and J. Wang, *J. Phys. Chem. Lett.*, 2021, **12**, 7221-7228.
10. P. Wang, Q. Shao, J. Guo, L. Bu and X. Huang, *Chem. Mater.*, 2020, **32**, 3144-3149.
11. J. Zhu, Y. Cen, H. Ma, W. Lian, J. Liu, H. Ou, F. Ouyang, L. Zhang and W. Zhang, *Nanoscale Horiz.*, 2023, **8**, 1273-1281.
12. Y. Qu, Z. Yu, D. Wei, L. Chen, Z. Zheng, N. Xiao, L. Wang and J. Yu, *Ionics*, 2021, **27**, 4885-4895.
13. T. Li, Y. Liu, R. Jia, M. Yaseen, L. Shi and L. Huang, *New J. Chem.*, 2021, **45**, 22327-22334.
14. G. Jiang, C. Zhang, X. Liu, J. Bai, M. Xu, Q. Xu, Y. Li, L. Long, G. Zhang, S. Li and Y. He, *Int. J. Hydrogen Energy*, 2022, **47**, 6631-6637.
15. A. Shan, X. Teng, Y. Zhang, P. Zhang, Y. Xu, C. Liu, H. Li, H. Ye and R. Wang, *Nano Energy*, 2022, **94**, 106913.
16. J. Han, C. Gong, C. He, P. He, J. Zhang and Z. Zhang, *J. Mater. Chem. A*, 2022, **10**, 16403-16408.
17. Z.-L. He, X. Huang, Q. Chen, C. Zhai, Y. Hu and M. Zhu, *J. Colloid Interf. Sci.*, 2022, **616**, 279-286.
18. N. Nie, D. Zhang, Z. Wang, Y. Qin, X. Zhai, B. Yang, J. Lai and L. Wang, *Small*, 2021, **17**, 2102879.
19. F. Shi, W. Wu, J. Chen and Q. Xu, *Chem. Commun.*, 2021, **57**, 7011-7014.
20. W. Zhao, C. Luo, Y. Lin, G.-B. Wang, H. M. Chen, P. Kuang and J. Yu, *ACS Catal.*, 2022, **12**, 5540-5548.